Limnol. Oceanogr., 57(1), 2012, 185–198

doi:10.4319/lo.2012.57.1.0185

Intensive and extensive nitrogen loss from intertidal permeable sediments of the Wadden Sea

Hang Gao,[a] Maciej Matyka,[a,1] Bo Liu,[a] Arzhang Khalili,[a,2] Joel E. Kostka,[a,3] Gavin Collins,[a,4] Stefan Jansen,[a,5] Moritz Holtappels,[a,*] Marlene M. Jensen,[a,6] Thomas H. Badewien,[b] Melanie Beck,[b] Maik Grunwald,[c] Dirk de Beer,[a] Gaute Lavik,[a] and Marcel M. M. Kuypers[a]

[a] Max Planck Institute for Marine Microbiology, Bremen, Germany
[b] Institute of Chemistry and Biology of the Marine Environment, University Oldenburg, Oldenburg, Germany
[c] Helmholtz-Zentrum Geesthacht, Geesthacht, Germany

Abstract

Nitrogen (N) loss rates were determined in permeable sediments of the Wadden Sea using a combination of stable N isotope incubation experiments and model simulation approaches during three seasons. Three different incubation methods that employed the isotope pairing technique were used: intact core incubations simulating either (1) diffusive or (2) advective transport conditions and (3) slurry incubations. N loss rates from core incubations under simulated advective transport conditions exceeded those rates measured under diffusive transport conditions by 1–2 orders of magnitude, but were comparable to those observed in slurry incubations. N loss rates generally showed little seasonal and spatial variation (207 ± 30 μmol m^{-2} h^{-1}) in autumn 2006 and spring and summer 2007. Utilizing an extensive time series of nutrient concentrations and current velocities obtained from a continuous monitoring station, nitrate and nitrite (i.e., NO_x^-) flux into the sediment was modeled over a full annual cycle. Fluxes were sufficient to support the experimentally derived N loss rates. Combining the measured rates with the modeled results, an annual N removal rate of 745 ± 109 mmol N m^{-2} yr^{-1} was estimated for permeable sediments of the Wadden Sea. This rate agrees well with previous N loss estimates for the Wadden Sea based on N budget calculations. Permeable sediments, accounting for 58–70% of the continental shelf area, are an important N sink and their contribution to the global N loss budget should be reevaluated.

Continental margin sediments represent a major sink of fixed nitrogen (N) in the oceanic N cycle (Gruber 2008; Thamdrup and Dalsgaard 2008). Benthic N_2 production in shelf sediments, derived from denitrification and anammox processes, accounts for 50–70% of fixed oceanic sedimentary N loss in current budgets (Gruber 2004; Codispoti 2007). Although the majority (58–70%) of continental margins are covered by coarse-grained relict sediments (Emery 1968; Johnson and Baldwin 1986), most previous biogeochemical research has focused on muddy or fine-grained shelf sediments, and the role of sandy sediments in N loss has been largely ignored.

The seafloor of the Wadden Sea, one of the largest tidal systems in the world, is dominated by permeable or sandy sediments. Recent studies showed that pore-water advection dominates chemical exchange at the sediment–water interface of the sandy seafloor, with advective transport exceeding the rate of molecular diffusion by several orders of magnitude (Precht and Huettel 2004). Pressure gradients driven by waves and currents interact with sediment topography (Precht and Huettel 2003), and pump solutes and particles from the overlying water into the sediment (Rusch and Huettel 2000; Reimers et al. 2004). Advective transport leads to an acceleration of organic matter mineralization and a stimulation of biogeochemical cycling proportional to the extent of pore-water exchange (De Beer et al. 2005). The high transport rates of organic matter and electron acceptors from the water column into the seafloor allow marine sands to act as an efficient filter for organic matter that may also facilitate N removal by denitrification. However, few studies have investigated N loss by denitrification in coastal permeable sediments (Lohse et al. 1996; Eyre and Ferguson 2002; Vance-Harris and Ingall 2005); and of these studies, few have incorporated advective transport processes.

Recent laboratory studies using ^{15}N-labeling experiments showed that denitrification rates in marine sands under simulated advective conditions are substantially enhanced relative to diffusive conditions (Cook et al. 2006; Rao et al. 2007; Gihring et al. 2010). Furthermore, rapid rates of denitrification (> 50 μmol m^{-2} h^{-1}) were measured under oxic conditions in permeable sediments affected by advection (Rao et al. 2007, 2008; Gao et al. 2010). These studies suggest that N loss in permeable sediments with advective pore-water flow is much higher than previously perceived. However, temporally and

* Corresponding author: mholtapp@mpi-bremen.de

Present addresses:
[1] Institute for Theoretical Physics, University of Wrocław, Wrocław, Poland
[2] Department of Earth and Environmental Sciences, Jacobs University Bremen, Bremen, Germany
[3] Department of Oceanography, Florida State University, Tallahassee, Florida
[4] Infrastructure and Environment, School of Engineering, University of Glasgow, Glasgow, United Kingdom
[5] Deltares, Utrecht, Netherlands
[6] Nordic Center of Earth Evolution (NordCEE) and Institute of Biology, University of Southern Denmark, Odense, Denmark

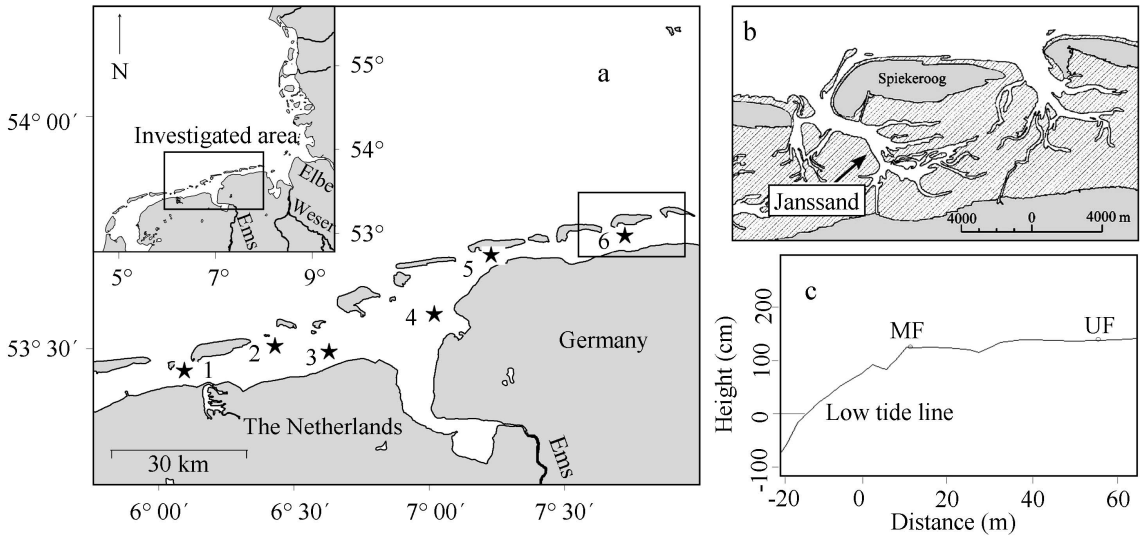

Fig. 1. (a) Intertidal sand flats sampled in 2006 along a transect in the East Frisian Wadden Sea. Stations labeled from 1 to 6 are Engelsmanplaat, Simonszand, Horsbornzand, Kopersand, Hohes Riff, and Janssand, respectively. (b) Location of Janssand (arrow), the primary sand flat studied. (c) A cross section of Janssand showing the elevation and the location of the sampling sites "middle flat" (MF) and "upper flat" (UF). The average water level at low tide (low-water line) is used as reference point for the height.

spatially resolved sedimentary N_2 production rates as well as estimates for the benthic NO_x pore-water flux have so far been missing.

In this study, we use a combination of ^{15}N-labeling experiments and a flux model based on annual monitoring data of NO_x concentrations and bottom current velocities to determine N loss from permeable sediments of the world's largest tidal system, the Wadden Sea. The consistency of measured N loss rates at different sites and during different seasons allows extrapolating the results to the entire Wadden Sea area. This study provides to our knowledge the first regional estimates of N loss from permeable sediments based on experimental data. Our results are comparable with N loss estimates for the Wadden Sea based on N budget calculations.

Methods

Study sites—The Wadden Sea, located in the southeastern part of the North Sea, stretches from Den Helder in the Netherlands in the southwest, past the great river estuaries of Germany, to its northern boundary at Skallingen north of Esbjerg in Denmark. The Wadden Sea covers 500 km of coastline, and encompasses a total area of about 14,700 km^2 (Fig. 1a). One-third of it is mainly composed of intertidal flats, and ~ 93% of the seafloor is covered by coarse, sandy, or mixed sediments (Common Wadden Sea Secretariat 2008).

Janssand is a typical intertidal sand flat in the central Wadden Sea that has been intensively studied as a hotspot of biogeochemical cycling (Jansen et al. 2009). The Janssand flat, located in the back barrier area of Spiekeroog Island in the German Wadden Sea (Fig. 1b), consists mainly of well-sorted sands with a mean grain size of 176 μm, porosities of 35% to 40%, and permeabilities ranging from 0.5 to 9.5 $\times$ 10^{-12} m^2 (Billerbeck et al. 2006). The eastern edge of the flat faces a 17-m-deep tidal channel separating the barrier islands Spiekeroog and Langeoog. The entire Janssand flat is inundated with ~ 2 m of seawater for 4–6 h during each semidiurnal tidal cycle and exposed to air for 6–8 h during low tide. Along the sloping margin from the central flat region to the low-water line, two representative sites were visited for detailed investigations of N loss processes using slurry incubations and intact core incubations simulating either diffusive or advective transport conditions (Table 1). An "upper flat" site (UF) is located ~ 80 m upslope, and a "middle flat" site (MF) lies in between the low-water line and UF (Fig. 1c). UF was chosen as a proxy for the central region, composed mainly of sandy sediments. The central tidal flat exhibits little to no incline, and its physical appearance is homogeneous. MF is along the edge of the tidal flat and in general entirely exposed during low tide. These two sites were investigated using the flat-bottom ships *Spes Mea* in October 2006 and *Doris von Ochtum* in March and August 2007.

To address the spatial variation of N loss processes throughout the Wadden Sea, we investigated additional five intertidal sand flats between the island Ameland (the Netherlands) and the island Spiekeroog (Germany) in October 2006 (Fig. 1a; Table 1). At all sites, sampling was conducted in the central region of the respective flats, and N loss rates were investigated using intact core incubation simulating advective transport conditions (*see* below).

Physical and chemical analysis—Time series measurements were performed at a station nearby the Janssand flat in the tidal inlet between the Islands Spiekeroog and Langeoog (Table 1). In situ temperature was determined from October 2006 to October 2007 using a temperature sensor (Pt100, 4H-JENA engineering GmbH) mounted at the time series station. For validation, conductivity, temperature, and depth measurements were conducted at regular intervals. Bottom-water current velocities were

Table 1. Summary of measurements at different study sites and seasons.

Sampling season	Sampling site	Measurement					
		DIN (NO_2^-, NO_3^-)	O_2	Current velocity	Intact core incubations		Slurry incubations tracer
					Tracer	Method	
Oct 2006	Engelsmanplaat	Site seawater and seawater amendment with tracer			$^{15}NO_3^-$	Percolation	
	Simonszand						
	Horsbornzand						
	Kopersand						
	Hohes Riff						
	Janssand upper flat			From current velocity data in Billerbeck et al. (2006)	$^{15}NO_3^-$	Percolation	
	Janssand middle flat		O_2 microsensor		$^{15}NO_3^-$	Percolation and diffusion	
Mar 2007	Janssand upper flat	Site seawater and seawater amended with tracer	O_2 microsensor	ADCP measurement in Apr 2010	$^{15}NO_3^-$	Percolation and diffusion	$^{15}NO_3^-$ with aerated seawater
	Janssand middle flat						
Aug 2007	Janssand upper flat	Site seawater and seawater amended with tracer	O_2 microsensor	ADCP measurement in Jul 2009	$^{15}NO_3^-$	Percolation and diffusion	$^{15}NO_3^-$ with aerated seawater
	Janssand middle flat						

measured using an acoustic Doppler current profiler (ADCP; 1200 KHz, Workhorse Sentinel, Teledyne RD Instruments) in July 2009 and April 2010. In July 2009, current velocities were monitored by a downward-looking ADCP mounted on a boat nearby the central Janssand. Flow velocities were measured from 80 cm above the sediment surface with a vertical resolution of 25 cm every 5 s for each ping. The same instrument was mounted upward looking on a bottom frame at the central Janssand flat over four tidal cycles in April 2010. For the upward deployments, the ADCP was mounted 9 cm above the seafloor and measured with a vertical resolution of 10 cm and a measuring interval of 10 s for 60 pings.

In parallel, real-time monitoring of NO_x^- concentration of near-surface water was conducted with an in situ automated nutrient analyzer (Systea, MicroMac1000; Grunwald et al. 2010) at the time series station. Concentrations of dissolved NO_3^- and NO_2^- were determined hourly after automated filtration using a loop-flow reactor and loop-flow analysis technology combined with conventional photometry (Grunwald et al. 2007). The detection limit for NO_x^- is ~ 0.2 μmol L^{-1} (Grunwald et al. 2010). For this study, a time series of NO_x^- data from October 2006 to October 2007 was used.

NO_x^- samples were also taken in parallel to the incubation experiments. At the sites and time periods when cores were collected for rate measurements, seawater was collected during low tide and filtered through a 0.2-μm syringe filter. Seawater was sampled before and after amendment with N isotope tracer. Pore-water sampling was performed in sediments during exposure, using a Rhizon method modified from Seeberg-Elverfeldt et al. (2005). A metal plate with holes at 1–1.4-cm intervals down to 15 cm was pushed into sediments. Rhizon samplers were inserted into the undisturbed sediments and mounted through the holes on the metal plate with only the sampling ports protruding from the sediments. In situ pore-water samples were directly extracted from these ports with sterile hypodermic syringes. All nutrient samples were frozen at -20°C immediately after sampling. NO_x^- was determined by chemiluminescence after reduction to NO with acidic vanadium(II) chloride (Braman and Hendrix 1989).

^{15}N labeling experiments—To investigate the N loss in permeable sediments of the Wadden Sea, the isotope pairing technique (IPT) (Hauck et al. 1958) has been applied in slurry incubations as well as in intact core incubations, simulating either diffusive or advective flow conditions.

The diffusive approach follows the protocol described by Nielsen (1992). For each experiment, 15 sediment cores were collected with Plexiglas push-cores (inner diameter, 3.5 cm; height, 28 cm). The water overlying the 10-cm-thick sediment cores was replaced with site seawater amended with $^{15}NO_3^-$ - to a final concentration of 50 μmol L^{-1}. The labeling percentages ranged from 41% to 99%. The cores were immediately sealed without any headspace by rubber stoppers and pre-incubated for 2 h at in situ temperature. During the incubations, the overlying water was continuously mixed by externally driven magnetic stirring bars at $\sim$ 60 revolutions per minute (rpm). After pre-incubation,

triplicate cores were destructively sampled at regular intervals (0, 1, 2, 4, and 6 h). Before sampling, 1 mL of zinc chloride ($ZnCl_2$) (50% w : v) was added to the sediment surface by opening each core lid stopper. The cores were immediately resealed without any headspace and mixed by inversion. After allowing sediment particles to settle, an aliquot of water for N_2 gas analysis was removed from each core and transferred to a 12-mL Exetainer™ (Labco), prefilled with 200 μL of saturated $HgCl_2$.

The advective approach is described by Gao et al. (2010) and De Beer et al. (2005). In detail, 15 sediment cores were collected in parallel to those used for the diffusive approach. The overlying water in each core was replaced with aerated site seawater amended with $^{15}NO_3^-$ - to a final concentration of 50 μmol L^{-1} (labeling percentages as described above). Rubber bottom and top stoppers of the cores were equipped with valves to allow the percolation of the overlying water through the sediment column. De Beer et al. (2005) used this method to continuously percolate water through the sediment column. In this study, the percolation was performed only once at the beginning of the experiment. Each core was rapidly percolated from top to bottom with 20 mL of labeled seawater, thus exchanging the pore water of the upper 5 cm of the sediment. The percolation of all 15 intact cores was performed within 25 min at an average flow of 12 mL min^{-1}. Subsequently, the cores were incubated at in situ temperature ($\sim$ 13°C in October 2006, $\sim$ 9°C in March 2007, and $\sim$ 20°C in August 2007) and destructively sampled in triplicate at regular intervals between 0 and 6 h (0, 1, 2, 3, and 4 h in summer and 0, 1, 2, 4, and 6 h in winter). The overlying water of all cores was mixed continuously at $\sim$ 60 rpm during the incubations by externally driven magnetic stirring bars. Cores were sacrificed in reverse order of percolation. Subsamples for rate determination were obtained in the same way as described in the diffusive approach.

Slurry incubations were performed at the Janssand sites as described by Gao et al. (2010) and N_2 productions were examined in gas-impermeable bags using ^{15}N tracer IPT according to Thamdrup and Dalsgaard (2002). Sediments were sampled using Plexiglas push-cores (inner diameter, 9.5 cm; height, 60 cm). The sediment core was sectioned into 2-cm-depth intervals to a depth of 6 cm. The sectioned sediment was transferred into gas-tight bags and mixed with air-saturated seawater from the study site at a volume ratio of 1 : 1.4. After removing the entire gas phase, the bags were sealed and $^{15}NO_3^-$ was injected through the rubber stopper into the bags to a final concentration of 200 μmol L^{-1} (labeling percentages ranged from $\sim$ 70% to $\sim$ 99%). Bags were mixed well and incubated at in situ temperature. During the incubation, the bags were periodically shaken to ensure a homogenous distribution of labeled N_2. Subsamples of the interstitial water were collected from the bags immediately before and after the addition of the tracer and at regular time intervals up to 16 h. The withdrawn subsamples were preserved in 6-mL Exetainer™ vials (Labco) without any headspace, each of which was prefilled with 100 μL of saturated $HgCl_2$.

Oxygen concentrations in slurry subsample were measured as described by Gao et al. (2010). Oxygen concentrations were measured directly after subsampling from the bags using oxygen microsensors. The sample vials were uncapped and a calibrated O_2 microsensor was inserted into the bottom of each vial for $\sim$ 10 s until the sensor signal stabilized. Sample vials were recapped immediately to avoid significant gas exchange.

^{15}N-N_2 measurements and rate calculations—A 1-mL helium headspace was introduced to each sample vial. The isotope ratios of dinitrogen gas ($^{29}N_2 : {}^{28}N_2$ and $^{30}N_2 : {}^{28}N_2$) in the headspace were determined by gas chromatography–isotope ratio mass spectrometry (GC-IRMS; VG Optima) by direct injection of the sample headspace. Concentrations of $^{30}N_2$ and $^{29}N_2$ were calculated from the excess relative to air according to Holtappels et al. (2011). Incubations without a significant linear trend in concentration over time ($p > 0.05$) were discarded. For further calculations we do not consider N loss via anammox since $^{29}N_2$ production in slurry incubations with added $^{15}NH_4^+$, $^{14}NO_3^-$, and allylthiourea was insignificant (data not shown here). It can be assumed that denitrification is the sole N loss process.

For intact core incubations using either the diffusive or advective approach, denitrification of $^{14}NO_3^-$ and $^{15}NO_3^-$ (D_{14} and D_{15}) is calculated from the production of $^{29}N_2 (p^{29}N_2)$ and $^{30}N_2 (p^{30}N_2)$ over the first 4 h (March) and 2 h (August) according to Nielsen (1992):

$$D_{15} = p^{29}N_2 + 2 \times p^{30}N_2 \quad (1)$$

$$D_{14} = \left[p^{29}N_2 / \left(2 \times p^{30}N_2\right)\right] \times \left(p^{29}N_2 + 2 \times p^{30}N_2\right) \quad (2)$$

We have strong arguments to assume that the advective NO_x^- transport from bottom waters into the first centimeters of the permeable sediment is not limiting denitrification under in situ conditions (*see* Discussion below). We therefore did not distinguish between D_{14} and D_{15} in the whole-core incubations. Thus, total N loss via denitrification (D_{tot}) is calculated as

$$D_{tot} = D_{14} + D_{15} \quad (3)$$

In slurry incubations, total N loss via denitrification (D_{tot}) is calculated from the production of $^{30}N_2$ over the first 4 h according to Thamdrup and Dalsgaard (2002):

$$D_{tot} = 2 \times p^{30}N_2 / (F_{15_{NO_3}})^2 \quad (4)$$

where $F_{15_{NO_3}}$ is the labeling percentage of nitrate. $F_{15_{NO_3}}$ is derived directly from the known amount of added $^{15}NO_3^-$ and the measured concentration of $^{14}NO_3^-$ in the added seawater:

$$F_{15_{NO_3}} = {}^{15}NO_3^- / \left({}^{14}NO_3^- + {}^{15}NO_3^-\right) \quad (5)$$

The initial labeling percentage ($F_{15_{NO_3}}$) may differ from the labeling percentage at a later time point ($F'_{15_{NO_3}}$) if the production of $^{14}NO_x^-$ via nitrification dilutes the initial labeling percentage. Assuming that denitrification is the only N loss process and that random isotope pairing of $^{14}NO_x^-$ and $^{15}NO_x^-$ leads to binomially distributed N_2

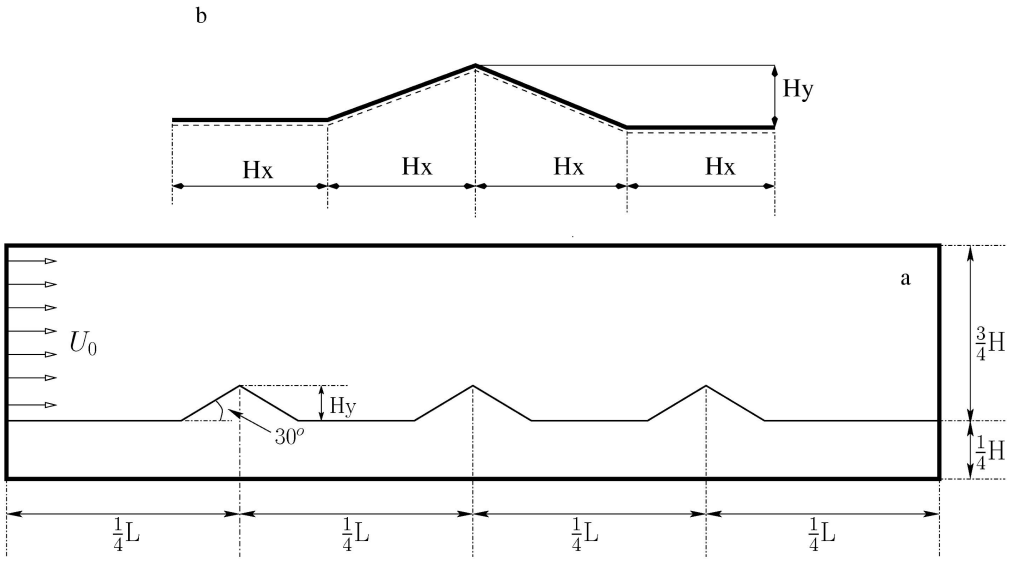

Fig. 2. (a) Schematic of the multiple ripples domain. The domain was composed of three ripples, and the slope of each ripple is assumed to be 30 degrees. The center points of three triangular ripples were located at ¼L, ½L, and ¾L beginning from the left. The vertical position of the interface line at the flat part was at ¼H. The inlet velocity was assumed to follow a uniform distribution U_0. (b) One ripple component. The dashed line represents the interface line. Hy is the height and 4Hx are the length of each ripple.

species $^{28}N_2$, $^{29}N_2$, and $^{30}N_2$ (Hauck et al. 1958; Nielsen 1992), $F'_{15_{NO_3}}$ can be calculated from the production of $^{29}N_2$ and $^{30}N_2$ according to

$$F'_{15_{NO_3}} = 2/(p^{29}N_2/p^{30}N_2 + 2) \quad (6)$$

Here, D_{tot} in slurry incubations (Eq. 4) was determined using $F'_{15_{NO_3}}$ instead of $F_{15_{NO_3}}$ with $p^{29}N_2$ and $p^{30}N_2$ calculated over the first 4 h. It should be mentioned that D_{tot} derived from combining Eqs. 4 + 6 is essentially equal to D_{tot} derived from combining Eqs. 1–3.

In the absence of anammox $F'_{15_{NO_3}}$ represents the actual labeling percentage of the denitrified NO_x^- pool during the incubation. A decrease of $F'_{15_{NO_3}}$ from the initial $F_{15_{NO_3}}$ indicates that the ^{15}N-labeling percentage was lowered during the incubation, most probably by the oxidation of $^{14}NH_4^+$ to $^{14}NO_x$ (nitrification). We discuss below if and to what extent any nitrification activity violates the IPT requirement of a constant labeling percentage.

Model of NO_x influx—Tidal flats in the Wadden Sea are dominated by highly permeable sandy sediments with rippled topography. Two dominant forces—waves and tidal currents—interacting with bottom topography, generate pressure gradients that drive the exchange of pore water with the overlying water. To simplify the model, only the force of tidal currents was incorporated. Due to the higher permeability, advective transport in sandy sediments exceeds the diffusive transport in the muddy sediments by orders of magnitude (Precht and Huettel 2004). Based on a two-dimensional single ripple model for permeable sediments presented by Huettel et al. (1996), a multiple rippled porous domain was constructed (Fig. 2a).

According to the topography of surface sediments at Janssand, the height of the ripple (Hy) was set to 2 cm, while the horizontal extent of a single ripple is divided into four equal lengths of Hx = 3.46 cm (Fig. 2b). The permeability and porosity of the sediment was obtained in measurements as $k = 10^{-12}$ m^2 and $\varphi = 0.39$, respectively. The inlet velocity (U_0) was taken in the range from 5×10^{-3} to 5×10^{-2} m s^{-1}. The fluid flow calculation in and above the sediment is based on the lattice Boltzmann method. Moreover, the velocity and pressure field were calculated from an extended Darcy equation (Guo and Zhao 2002).

For the computation of the velocity and pressure field, the hydrodynamics of percolation is characterized by the Reynolds number, Re, here defined by the equation:

$$Re = U_0 \times Hy \times \nu^{-1} \quad (7)$$

The symbol ν in Eq. 7 denotes the kinematic viscosity of the seawater, which is a function of temperature, T (in °C). The relationship between ν and T can be expressed by the following equation (Kampmeyer 1952; Perry and Green 1984):

$$\nu = 1.35 \times 2.5^{(-0.047T)} + 0.435 \quad (8)$$

where ν has the unit of 10^{-6} m^2 s^{-1}. Revealed from the computation results, the flow shows an unsteady nature when Re is > 100 ($U_0 > 5 \times 10^{-3}$ m s^{-1}). Therefore, an averaging procedure for velocity fields was performed over $\sim 10^7$ time steps, equivalent to 1 h. The convergence criterion is the time-independent average inward flow velocity (U_{in}), which was defined as a sum of velocity components normal to the interface line. In order to avoid overestimation of the flux due to high velocities close to the interface line, U_{in} was calculated a few lattice nodes below the interface (dashed line in Fig. 2). Calculations were carried out for a range of Reynolds numbers, Re = 100, 200, 400, 600, and 1000 with the corresponding U_0 = 0.5, 1, 2, 3, 5×10^{-2} m s^{-1}. For a given range of parameters it was

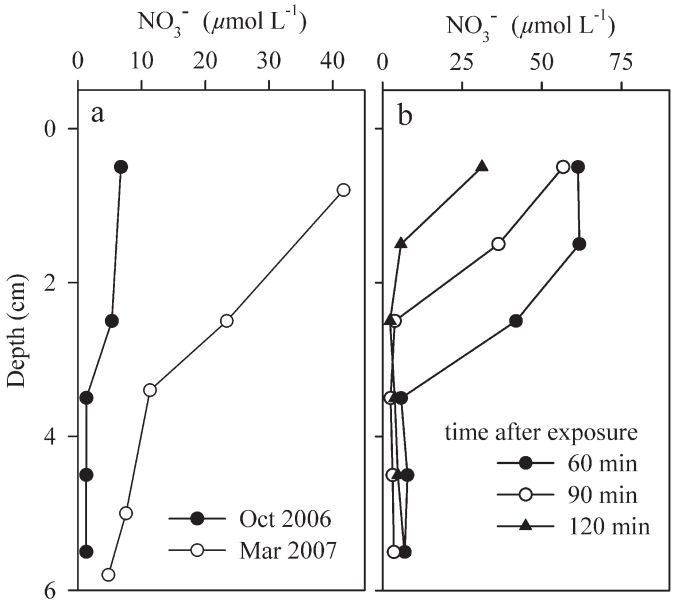

Fig. 3. (a) NO_3^- concentrations in the pore water during the first hour of exposure in October 2006 and March 2007. (b) Consecutive NO_3^- pore-water measurements during the first 1.5 h of exposure in March 2007. (a, b) The measurements in March 2007 were made at different days. The measurement site is Janssand, middle flat.

found that U_{in} can be expressed as an exponential function of the Reynolds number using the equation:

$$U_{in} = a \times Re^b \quad (9)$$

The fitting procedure gave $a = 2.57 \times 10^{-10}$ (m h^{-1}) and $b = 2.62$ and a similar equation was also reported to confirm our modeled results (Cardenas and Wilson 2007). This relation was used to extrapolate U_{in} to higher Reynolds numbers in order to cover the full range of current velocities measured at Janssand.

Assuming advective transport from the water column into the sediment (U_{in}) and a constant NO_x^- concentration in the overlying water (C_N), the inward advective NO_x^- flux (F_N) across the water–sediment interface is expressed by:

$$F_N = U_{in} \times C_N \quad (10)$$

Results

NO_x pore-water profiles—Representative results of NO_x^- concentrations in the pore water during the first 1–2 h of exposure are shown in Fig. 3a,b. In October 2006, NO_x^- concentrations in the pore water decrease from 7 μmol L^{-1} at the surface to 1 μmol L^{-1} at 3.5-cm depth (Fig. 3a). In March 2007, NO_x^- concentrations decrease from 42 μmol L^{-1} at the surface to 5 μmol L^{-1} at 5.8-cm depth (Fig. 3a). The dynamic change of NO_x^- concentration over time is exemplified by consecutive pore-water measurements (Fig. 3b). Because pore water is stagnant during times of exposure, the NO_x supply from the bottom water ceased and NO_x-consuming processes cause the rapid decrease of NO_x^- concentrations during the first 80 min of exposure. NO_x^- consumption calculated from these pore-water profiles was 1.2 mmol N m^{-2} h^{-1}.

N loss from sediment core and slurry incubations—Constant production of $^{29}N_2$ and $^{30}N_2$ over the first 4 h was observed in all core incubations under simulated diffusive as well as advective transport conditions (representative results shown in Fig. 4a,b). Under diffusive transport conditions, the observed total N loss rates (D_{tot}) ranged from below detection to 19 ± 7 μmol N m^{-2} h^{-1}. Under simulated advective transport conditions, N loss rates were consistently 1–2 orders of magnitude higher (169–238 μmol N m^{-2} h^{-1}) (Table 2). In slurry incubations, oxygen was present during the first 4–6 h in March and during the first 1–2 h in August (representative results shown in Fig. 4c,d). Despite the initial presence of O_2, a constant production of $^{29}N_2$ and $^{30}N_2$ was observed during all seasons, consistent with the previous findings of Gao et al. (2010). N loss rates obtained from slurry incubations ranged between 144 and 303 μmol N m^{-2} h^{-1} when integrated over the upper 5-cm depth, and largely agreed with rates measured in percolated sediment cores (Table 2).

Spatial and temporal variability of benthic N loss—The temporal and spatial variability of N loss rates measured either in slurries or percolated cores was minor. In March 2007, the N loss rates in percolated cores were slightly higher at the upper flat in comparison to the middle flat (230 and 169 μmol N m^{-2} h^{-1}, respectively), while in August 2007 the N loss rates were not significantly different between the same sampling sites (188 and 209 μmol N m^{-2} h^{-1}, respectively). In March and August 2007, N loss rates obtained from slurry incubation were comparable to those obtained from percolated cores and showed similar deviations between the sampling sites (Table 2). In general, N loss rates between the upper and middle flat in the three field campaigns were consistent (on average ~ 200 μmol N m^{-2} h^{-1}) with the exception of the N loss rate measured in the middle flat in October 2006, which was 5-fold increased. However, at the same time the N loss rate at the upper flat was 238 μmol N m^{-2} h^{-1}, which was again similar to rates measured in March and August 2007 (Table 2).

In October 2006, N loss rates were investigated at six stations along a transect through the East Frisian Wadden Sea. The rates were similar to those measured at Janssand, ranging from 176 to 289 μmol N m^{-2} h^{-1} (Table 3). The rates at the eastern stations (Sta. 3–6) were slightly increased compared to western stations (Sta. 1 and 2) (Fig. 1a). However, the variation along the 100-km transect was small. In summary, at the transect sites and during the three sampling campaigns at Janssand (Tables 2, 3), N loss rates in percolated cores varied by less than a factor of 2 (with the exception of the high rate at the middle flat in October 2006).

Modeled NO_x^- fluxes from overlying water into permeable sediments—Current velocities at 10–50 cm above the sediment were measured in July 2009 and April 2010.

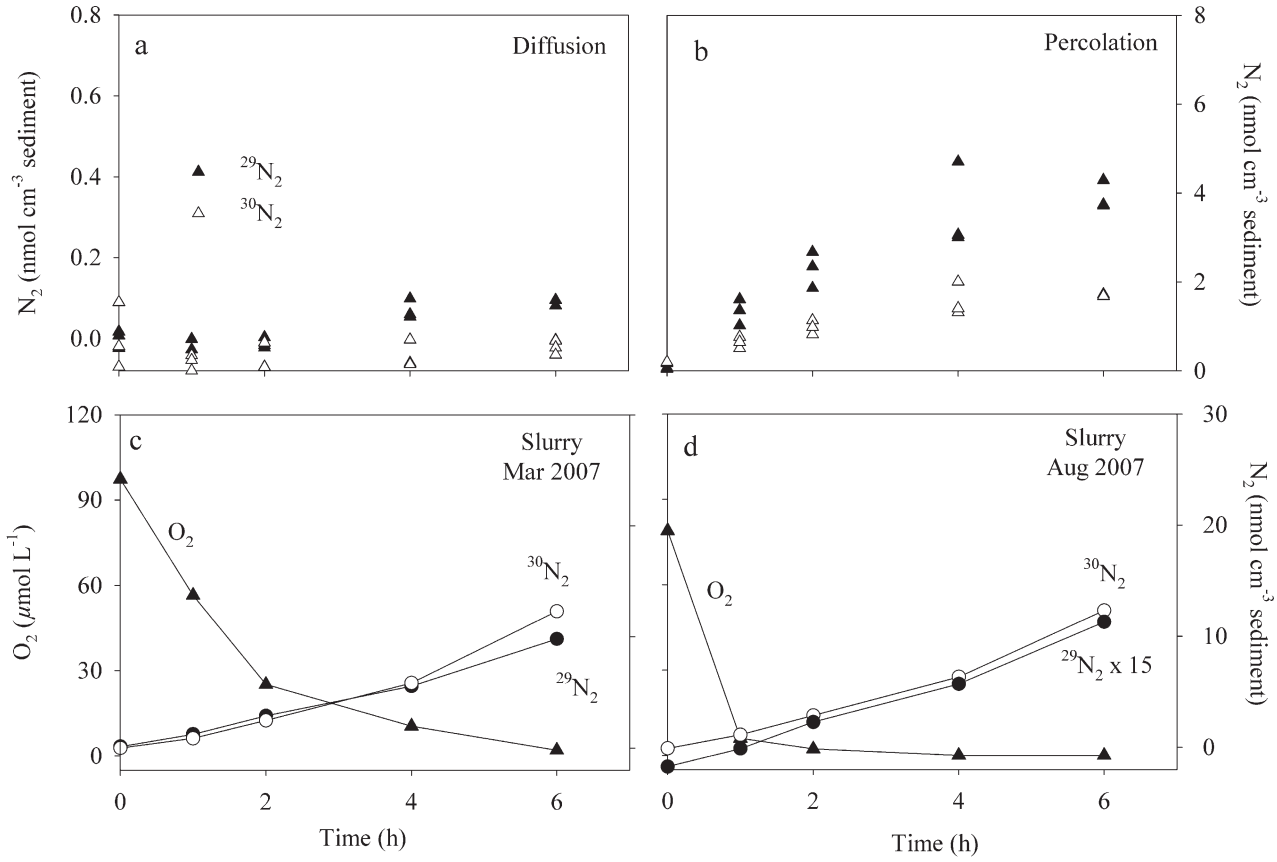

Fig. 4. $^{29}N_2$ and $^{30}N_2$ concentration over time in intact core incubations simulating (a) diffusive conditions and (b) advective conditions in March 2007. Labeled N_2 and oxygen concentration over time in slurry incubations of the upper sediment (0–2 cm) in (c) March 2007 and (d) August 2007. Note that $^{29}N_2$ in panel d was multiplied by 15 to fit the same scale.

Table 2. N loss rates determined from intact core and slurry incubations at Janssand.

		N loss rate (μmol m^{-2} h^{-1}) ± standard error		
Sampling season	Sampling site	Intact core incubation diffusion	Intact core incubation percolation (down to 5 cm)	Slurry incubation (integrated to 5 cm)
Oct 2006	Upper flat	—	238.4±41.8	—
	Middle flat	9.5±0.4	1056.2±162.6	—
Mar 2007	Upper flat	4.7±0.7	230.0±24.0	303.4±10.2
	Middle flat	Not detectable	168.9±13.7	144.2±11.8
Aug 2007	Upper flat	18.9±7.1	188.5±43.7	179.3±7.0
	Middle flat	8.6±1.3	209.2±28.9	262.1±24.5

Table 3. N loss rates determined at sand flats along a transect in the East Frisian Wadden Sea.

Sampling season	Site No.	Site name	Latitude, longitude	N loss rates (μmol N m^{-2} h^{-1}) ± standard error
Oct 2006	1	Engelsmanplaat	53°26.2′N, 06°04.4′E	175.9±57.4
	2	Simonszand	53°30.3′N, 06°25.3′E	185.1±14.2
	3	Horsbornzand	53°29.17′N, 06°39.46′E	236.9±8.4
	4	Kopersand	53°34′N, 07°01′E	288.6±51.0
	5	Hohes Riff	53°41.5′N, 07°12.7′E	255.6±101.1
	6	Janssand	53°44.11′N, 7°41.95′E	238.4±41.8

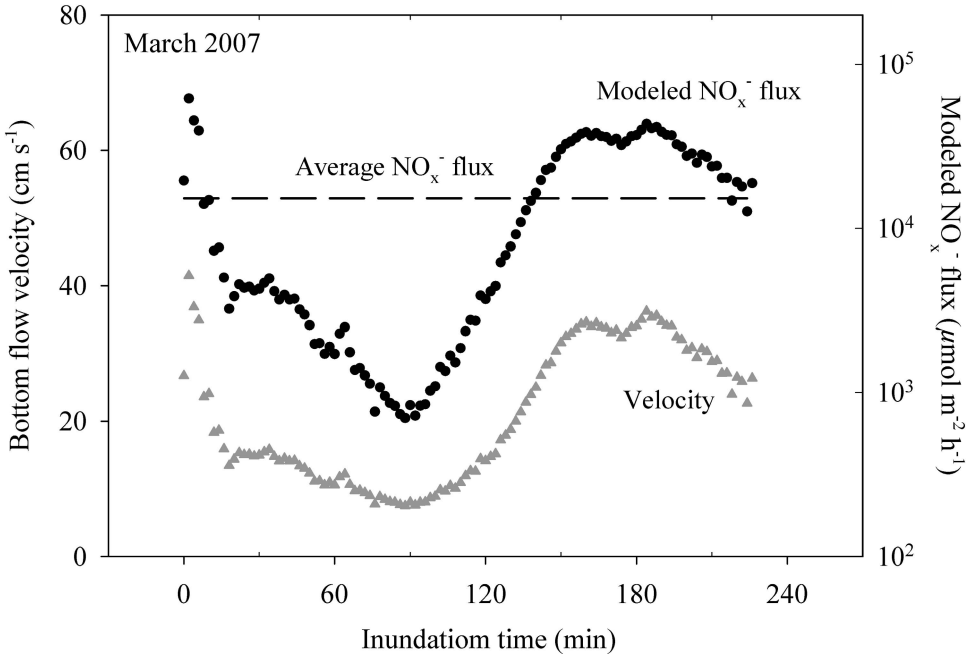

Fig. 5. An example of modeled NO_x^- flux as a function of bottom flow velocity during inundation. The velocities in this plot (gray triangles) represent average values measured over four tidal cycles in April 2010. Modeled NO_x^- fluxes (black dots) were obtained from Eq. 10 using average NO_x^- concentrations (32.7 μmol L^{-1}) and temperatures (7.3°C) of the bottom water in March. The average NO_x^- flux (dashed line) was calculated from the modeled NO_x^- flux over one inundation period.

The velocities presented in Fig. 5 were measured in April 2010 and averaged over four complete inundation periods (about 4 h of a full tidal cycle). During the rising tide, an initial current velocity of 41.5 cm s^{-1} was measured, which decreased to a minimum of 7.6 cm s^{-1} at high tide. At falling water level, the current velocity increased to a maximum of 36 cm s^{-1} and, thereafter, decreased to 25 cm s^{-1} during the last hour of inundation. Current velocities during the individual inundation periods were consistent and comparable to current velocity measurements in July 2009. In general, current velocities in the Wadden Sea are governed by tidal forces and wind, and show little seasonal variation with the exception of storm events (Badewien et al. 2009). Hence, the averaged values presented in Fig. 5 were used as U_0 to calculate the inward flow velocities into the sediment (U_{in}) from Eqs. 7–9.

In general, NO_x^- concentrations in the water column nearby Janssand exhibited a strong seasonal variability. NO_x^- concentrations ranging from below 1 to up to 110 μmol L^{-1} were measured by Grunwald et al. (2010) between January 2006 and December 2008. For the model, NO_x^- concentrations measured between October 2006 and October 2007 were applied. Concentrations were negatively correlated with temperature, but positively correlated with the loading of dissolved inorganic nitrogen estimated previously from riverine input (Grunwald et al. 2010). In winter 2006 and early spring 2007, daily averaged NO_x^- concentrations in the water column increased to maximum values of 40 μmol L^{-1}. During early summer, the NO_x^- concentrations declined rapidly to values of around 1 μmol L^{-1}. NO_x^- concentration then gradually increased to 5–10 μmol L^{-1} in the late summer and autumn.

Measured NO_x^- concentrations (C_N) and modeled inward flow velocities (U_{in}) were used to calculate the NO_x^- flux (F_N) over a full inundation period according to Eq. 10. An example of modeled NO_x^- fluxes in March 2007 is shown in Fig. 5. There, the mean NO_x^- concentration and temperature were applied (32 μmol L^{-1} and 7.3°C, respectively), and therefore, the simulated NO_x^- flux is responding to the current velocity only (*see* Eqs. 7–10). The estimated NO_x^- flux into the sediments was 700 μmol m^{-2} h^{-1} at low velocities and increased to 4.3 $\times$ 10^4 μmol m^{-2} h^{-1} at maximum velocities. The NO_x^- flux averaged over the full inundation period was 1.5 $\times$ 10^4 $\pm$ 3.0 $\times$ 10^3 μmol m^{-2} h^{-1} (Fig. 5).

Over the seasonal cycle, modeled NO_x^- flux is a function of the availableNO_x^- concentration in the overlying water (Fig. 6b). For example, increased NO_x^- concentration of 48.0 μmol L^{-1} in March 2007 with the temperature of 7.6°C caused the modeled NO_x^- flux to increase to 2.3 $\times$ 10^4 μmol m^{-2} h^{-1}. In contrast, although the temperature increased by a factor of > 2 in October 2006 and August 2007, decreased NO_x^- concentrations of $\sim$ 0.7 μmol L^{-1} resulted in modeled NO_x^- fluxes of $\sim$ 700 μmol m^{-2} h^{-1}. Over the experimentally investigated seasons, modeled NO_x^- fluxes into permeable sediments were at least 2 times higher than the measured denitrification rates (Fig. 6; Table 2).

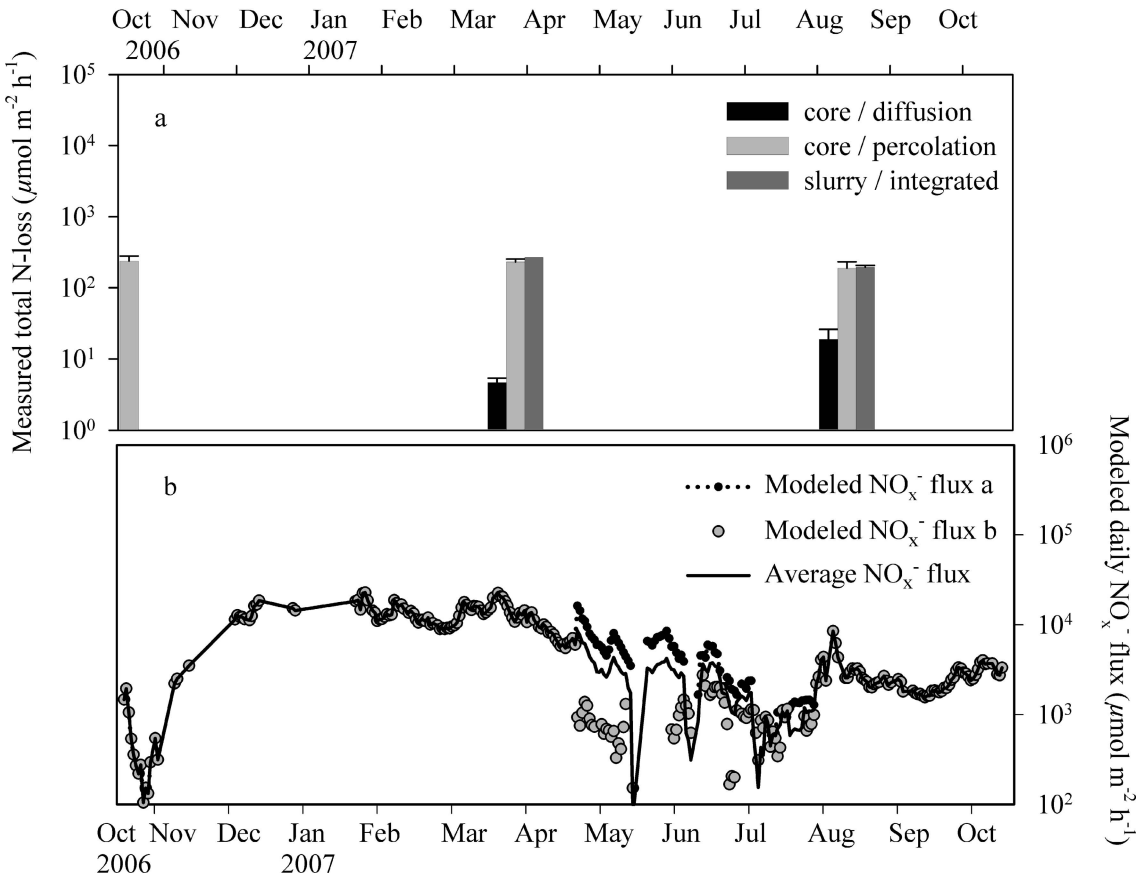

Fig. 6. N loss rates and NO_x^- fluxes determined from October 2006 to October 2007. (a) N loss rates measured at the upper flat at Janssand using different incubation methods. (b) Modeled NO_x^- fluxes derived from ambient NO_x^- concentrations, which were measured at the time series station over the same time period. In place of missing data from April to July in 2007, the data from the same time period in 2006 (black dots) and in 2009 (gray dots) were shown in the figure. The average NO_x^- concentrations from April to July of both years were used to model the mean NO_x^- fluxes (black line) over the annual cycle. (a, b) Note the different scales.

Discussion

N loss from diffusive core incubations—In several previous studies, denitrification in permeable sediments was investigated by simulating diffusive transport conditions. Denitrification rates measured in these studies varied widely up to 133 μmol N m^{-2} h^{-1} (Table 4). In this study, N loss rates obtained from intact cores under diffusive transport conditions (< 19 μmol N m^{-2} h^{-1}; Table 2) were in the range of previously reported rates from the Wadden Sea permeable sediments (1–42 μmol N m^{-2} h^{-1}; Table 4). In contrast, N loss rates obtained from intact cores under advective transport conditions (on average ~ 200 μmol N m^{-2} h^{-1}) were 1–2 orders of magnitude higher than those measured under diffusive flow conditions at the same sampling sites (Table 2). The increased N loss under advective conditions was consistent with findings from permeable sediments in the South Atlantic Bight, where diffusive core incubations (Vance-Harris and Ingall 2005) and advective core incubations (Rao et al. 2007) from the same site deviated by 1–2 orders of magnitude. In this study, rates from percolated core incubations substantially exceed most denitrification rates reported from the northern coastal muddy sediments in Europe (Table 4) but agree well with the previous studies that observed enhanced N loss rates due to advective transport in permeable sediments (Cook et al. 2006; Rao et al. 2007; Gihring et al. 2010).

N loss from slurries and percolated core incubations—O_2 dynamics in permeable Wadden Sea sediments are largely influenced by advective pore-water flow driven by waves and bottom-water currents over uneven topography. Variable pressure gradients, caused by ripple migration, waves, and variable currents, and the presence and absence of bottom-water currents during times of inundation and exposure directly affect the pore-water flow and thus the availability of oxygen and nitrate in the sediment. During inundation, advective pore-water flow causes deep penetration of O_2 (~ 5 cm) (Billerbeck et al. 2006; Jansen et al. 2009), thus enlarging the oxic and suboxic biogeochemical zone and enhancing the remineralization rate of organic matter (De Beer et al. 2005). The oscillation between deep and shallow O_2 penetration depths during times of inundation and exposure may also favor the overlap of oxic and anoxic processes. Indeed, Gao et al. (2010) and Rao et al. (2007) reported substantial denitrification rates occurring in aerobic permeable surface sediments.

Table 4. Denitrification rates reported for coastal marine environments.

Location	Sediment type	Method	Denitrification rate (μmol N m^{-2} h^{-1})	Reference
Texel, Wadden Sea	Sand	Acetylene block method	0.9–42	Kieskamp et al. 1991
Southern North Sea	Fine sand	Acetylene block method	5.8–8.9	Lohse et al. 1996
	Fine sand	$^{15}N_2$ isotope pairing method	8.9–11.9	Devol 1991; Lohse et al. 1996; Laursen and Seitzinger 2002
Svalbard	Fine sand	N_2 flux	33.6	Devol et al. 1997
Mid-Atlantic Bight	Sand	N_2 flux	68.8	Laursen and Seitzinger 2002
Washington State shelf	Sand	N_2 flux	133.3	Devol 1991
North Sea	Sand and mud	NO_3^- consumption model	28.6	Billen 1978
Baltic Sea	Sand and mud	Geochemical model	93.4	Shaffer and Rönner 1984
	Sand and mud	$^{15}N_2$ isotope pairing method	0.5–4.5;13.4–28.7	Deutsch et al. 2010
Northern Baltic Proper Gulf of Finland	Mud	$^{15}N_2$ isotope pairing method	0–12.5 3–26.8	Tuominen et al. 1998
Aarhus Bay	Silt	$^{15}N_2$ isotope pairing method	12.2–20.8	Nielsen and Glud 1996

Furthermore, the advective pore-water flow causes the deep penetration of NO_x^- into the sediment. Pore-water profiles show that NO_x^- is still available at sediment depths of up to 6 cm (Fig. 3a). When the influx of NO_x^- ceases during exposure, consecutive pore-water measurements show a rapid decrease of NO_x^- concentrations (Fig. 3b), indicating high NO_x^- consumption. NO_x^- consumption calculated from these pore-water profiles was 6-fold higher (1.2 mmol N m^{-2} h^{-1}) compared to the average N loss measured in slurry and percolated core incubations (0.2 mmol N m^{-2} h^{-1}). This suggests that the results from slurry and percolated core incubations may even underestimate the in situ N loss under natural conditions.

The dynamic nature of pore-water advection complicates the investigation of N cycling in permeable sediments. Experiments used in this study, i.e., the incubation of slurries and percolated cores, aim to mimic a period of inundation when oxygenated and nitrate-containing bottom water is injected into the sediment, followed by a period of exposure during which pore water is stagnant and O_2 is consumed until anaerobic conditions prevail. Under the initial oxic incubation condition, it can be expected that nitrification constantly adds $^{14}NO_x^-$ to the NO_x^- pool, resulting in the decrease of $^{30}N_2$ relative to $^{29}N_2$ production over time. This would violate the steady-state assumption behind the IPT method, which requires a constant labeling percentage over time. However, during the first 4 h of slurry and percolated core incubations no change of $^{30}N_2$ and $^{29}N_2$ production was observed (Fig. 4). In percolated core incubations this can be explained by the fact that the initial oxygen was rapidly consumed within the first 30 to 60 min of the incubation, i.e., between subsampling at 0 and 1 h (Gao et al. 2010; Fig. 3). Hence, a change of the NO_x^- labeling percentage can be expected only in the first hour of the incubation. Thereafter, steady-state labeling percentage can be assumed. Likewise, steady-state conditions are assumed in the slurry incubations in August 2007, when O_2 was consumed within the first 90 min (Fig. 4d). Finally, the oxygen consumption in the first hour of the incubation resulted in only minor changes of the labeling percentages. The decrease of $F'_{15_{NO_3}}$ (Eq. 6) relative to $F_{15_{NO_3}}$ (Eq. 5) was on average below 5% in the percolated core incubations and below 3% in the slurry incubations in August 2007.

In percolated core incubation, microbial cell densities remain unaffected, while cell densities in slurry incubations are diluted and, assuming constant cell specific respiration rates, the change from oxic to anoxic condition may last longer. This was the case in March 2007, when oxic conditions in slurry incubations lasted for up to 6 h (Fig. 4c). Nevertheless, N_2 production was constant within this period because most of the initial oxygen (starting concentration $\sim$ 300 μmol L^{-1}) was consumed before the first subsampling, which resulted in a decrease of the initial labeling percentage ($F'_{15_{NO_3}}$ compared to $F_{15_{NO_3}}$) of 15% on average. Thereafter, the contribution of nitrification to the $^{14}NO_3^-$ pool was most likely insignificant. The potential error was estimated by calculating the amount of nitrified $^{14}NO_3^-$ from the O_2 consumed during the incubation (between 90 and 30 μmol L^{-1}) assuming an $O_2 : NO_3^-$ ratio of 138 : 16 (Jahnke et al. 1982). The maximum potential decrease in labeling percentage was 3.3%, resulting in an increase of D_{tot} (Eq. 3) of $< 7\%$. In summary, we assume the labeling percentage of the NO_x^- pool to be in steady state in slurry and percolated core incubations—despite the initial dynamic oxygen regime.

NO_x^- availability under in situ conditions—Low N loss rates measured under diffusive transport conditions are likely limited by NO_x^- availability. As diffusive transport conditions are not realistic in permeable surface sediments (Huettel et al. 1996, 1998), this limitation was overcome in core incubations where $^{15}NO_3^-$-enriched bottom water was percolated through the sediment. In percolated core incubations as well as in slurry incubations, N substrate was available throughout the incubation and therefore

Table 5. Annual N loss determined for the sandy seafloor of the Wadden Sea.

(a) Intertidal sand flats

	N loss rate (μmol N m^{-2} h^{-1})	Inundation time		N loss rate integrated over inundation time and year (mmol N m^{-2} per 3600 h)	Annual N loss rate (mmol N m^{-2} yr^{-1})
		Hours per day	Days per year		
Experimental average	207.0±30.4	10	360	745.2±09.4	745.2±109.4
Modeled NO_x^- flux	<207.0±30.4	10	5	—	

(b) Other areas where sands dominate the seafloor

Geomorphological region of the Wadden Sea	Area (km^2)	Percentage of sandy permeable sediments (%)	Annual N loss rate (mmol m^{-2} yr^{-1})	N loss estimate ($\times$ 10^6 kg N yr^{-1})
Intertidal flats	4700	93	745.2±109.4	45.6±6.7
Subtidal flats and gullies	3700	80 (almost all)	1788.5±262.6	74.1±10.9
Offshore area	4900	80 (almost all)	1788.5±262.6	98.2±14.4

denitrification rates were not N limited and may be considered as potential rates. However, we provide the following arguments suggesting that in situ denitrification rates are most of the year not N limited in the first centimeters of permeable sediments.

At the same study site, repeated observations of deep O_2 penetration of several centimeters indicate significant advective transport of bottom water into the sediment (Billerbeck et al. 2006; Jansen et al. 2009). This advective transport stimulated oxygen consumption rates to increase 1–2 orders of magnitude (De Beer et al. 2005)—similar to the observed increase of denitrification in this study. In addition, NO_x^- was detected in pore waters down to depths of 6 cm and more (Fig. 3; Gao et al. 2010). The NO_x^- profiles were consistent with the modeled NO_x^- fluxes, which were sufficient during most of the year to support the measured N loss rates. The modeled NO_x^- fluxes are conservative estimates since NO_x^- flux due to wave motion and bioirrigation and the NO_x^- contribution from nitrification was not considered. Furthermore, in all rate measurements we observed the immediate start of a constant production of labeled N_2 (Fig. 4). Any adaptation to increased N substrate availability, on either cell or community level, would have resulted in an initial lag phase of the N_2 production.

We also assume that the denitrifying community is well adapted to variable and in particular to low NO_x^- concentrations. First of all, the measured N loss rates were similar in all slurry and percolated core incubations, although the background nitrate concentrations differed by $>$ 80 μmol L^{-1}. Further evidence comes from experiments, in which Gao et al. (2010) used microsensors to measure NO_x^- consumption in a sediment core after percolation of bottom water. They observed a decrease of NO_x from 60 μmol L^{-1} down to submicromolar concentrations without significant change of rates, suggesting that denitrification activity is not affected by low NO_x^- concentrations, such as those measured in the bottom water during summer. In summary, we suggest that N loss rates from percolated core incubations provide reasonable estimates for in situ denitrification rates, while diffusive core incubations are inadequate because advective pore-water transport is not considered.

Consistency of temporal and spatial N loss—N loss rates obtained from advective core incubations were very similar at different sampling sites and throughout the different sampling periods (168 to 288 μmol m^{-2} h^{-1}; Table 2), although the background NO_x^- concentrations and the modeled NO_x^- influxes were highly variable. The factors responsible for the consistent N loss rates in the permeable sediments of the Wadden Sea remain speculative. The input or availability of organic carbon as a substrate for heterotrophic denitrification could potentially have limited the N loss rates as has been shown in previous studies (Trimmer and Nicholls 2009). However, one would expect organic carbon concentration to be variable rather than uniform during the different sampling seasons. Alternatively, the consistent N loss rate could depend on the capacity of permeable sediment to host a microbial community. Compared to impermeable sediments with higher porosity and diffusive pore-water transport, microorganisms in permeable sediments can colonize only the surface of the sand grains, since the pore space is exchanged with the pore-water flow, which leads to fewer microorganisms per cubic centimeter. However, elucidating the causes for this consistency is beyond the scope of this work and has to be investigated in future studies.

Annual N loss from permeable Wadden Sea sediments—Based on the constant N loss rates during the different sampling periods and at the various sampling sites (Tables 2, 4) we estimated the annual N loss from permeable Wadden Sea sediments. The inundation periods of the studied intertidal sediments were 8–12 h d^{-1} (i.e., 4–6 h per cycle) with a mean of 10 h d^{-1} (Table 5a). Since no substantial difference was observed between N loss rates from percolated core and slurry incubations (Table 2), we used an average areal N loss of 207 μmol N m^{-2} h^{-1} derived from percolated core incubations. Integrating these

rates over the annual cycle, we assumed the areal N loss to take place whenever the modeled NO_x^- fluxes were sufficient, i.e., higher than the measured rates. This was the case for 360 d of the year. For the remaining 5 d, modeled NO_x^- fluxes were lower than the experimentally derived N loss and therefore rates during these days were conservatively set to zero. In summary, the annual N loss per square meter from the intertidal sand flats of the Wadden Sea is 745 $\pm$ 109 mmol N m^{-2} yr^{-1} (Table 5a), which is comparable to the mean annual N loss rate of $\sim$ 600 mmol N m^{-2} yr^{-1} estimated previously for the entire seafloor area of the Wadden Sea (van Beusekom et al. 2008).

One-third of the Wadden Sea area ($\sim$ 4700 km^2) is composed of sandy intertidal sediments (Common Wadden Sea Secretariat 2008). Based on our annual N loss rate and the intertidal area, the annual N removal from intertidal flats of the Wadden Sea is calculated to be 46 $\pm$ 7 $\times$ 10^6 kg N yr^{-1} (Table 5b). Furthermore, the subtidal flat areas (3700 km^2) and offshore areas (4900 km^2) are to a large extent covered by coarse permeable sediments (Common Wadden Sea Secretariat 2008), in which comparable advective pore-water transport and oxygen penetration depths were observed (Janssen 2004). We conservatively estimated that 80% of the subtidal Wadden Sea area is covered by permeable sediments. From the observed consistency of N loss in the intertidal zones of Wadden Sea sediments, a similar N loss of 207 μmol N m^{-2} h^{-1} was assumed for the subtidal zones. Given that the subtidal zone is continuously inundated, the annual N loss per square meter in subtidal and offshore areas is estimated to be 1788 $\pm$ 263 mmol N m^{-2} yr^{-1} (Table 5b). Integrating over all intertidal and subtidal areas, the annual N loss from permeable sediments of the entire Wadden Sea adds up to 218 $\pm$ 32 $\times$ 10^6 kg N yr^{-1} (Table 5b), which exceeds the previously reported estimate of $\sim$ 112 $\times$ 10^6 kg N yr^{-1} (van Beusekom et al. 2008), and accounts for $\sim$ 30% of the total annual N input into the Wadden Sea (745 to 820 $\times$ 10^6 kg N yr^{-1}; van Beusekom et al. 2001). These results underline the importance of the sandy Wadden Sea seafloor as a major sink for riverine N loads that enter the German Bight.

Permeable sediments are widespread in coastal areas and account for up to 70% of the shelf sediments (Johnson and Baldwin 1986). However, the mean annual N loss from shelf sediments is currently estimated to be $\sim$ 146 mmol N m^{-2} yr^{-1} (Galloway et al. 2004), which is only one-fifth of the areal rates measured in this study. Therefore, the contribution of permeable sediments to the N loss from shelf sediments should be reevaluated, and the high potential of permeable sediments to regulate the flow of nitrogen at the land–sea boundary should be further investigated.

Acknowledgments

We thank Hans Roy, Frank Schreiber, Ingrid Dohrmann, and Hani Tahsk for their field support, and Gabriele Klockgether and Daniela Franzke for their technical support in the lab. We are grateful to Ronald Monas and Ole Pfeiler for the ship time and excellent collaboration. We thank the reviewers for their constructive comments and suggestions. This research was funded by the Max Planck Society (MPG) and the German Research Foundation (DFG). HG was supported by the scholarships from German Academic Exchange Center (DAAD) and MPG.

References

Badewien, T. H., E. Zimmer, A. Bartholomä, and R. Reuter. 2009. Towards continuous long-term measurements of suspended particulate matter (SPM) in turbid coastal waters. Ocean Dynam. **59:** 227–238, doi:10.1007/s10236-009-0183-8

Billen, G. 1978. A budget of nitrogen recycling in North Sea sediments off the Belgian Coast. Estuar. Coast Mar. Sci. **7:** 127–146, doi:10.1016/0302-3524(78)90070-1

Billerbeck, M., U. Werner, L. Polerecky, E. Walpersdorf, D. De Beer, and M. Huettel. 2006. Surficial and deep pore water circulation governs spatial and temporal scales of nutrient recycling in intertidal sand flat sediments. Mar. Ecol. Prog. Ser. **326:** 61–76, doi:10.3354/meps326061

Braman, R. S., and S. A. Hendrix. 1989. Nanogram nitrite and nitrate determination in environmental and biological-materials by vanadium(iii) reduction with chemi-luminescence detection. Anal. Chem. **61:** 2715–2718, doi:10.1021/ac00199a007

Cardenas, B. M., and L. J. Wilson. 2007. Dunes, turbulent eddies and interfacial exchange with permeable sediments. Water Resour. Res. **43:** 1–16.

Codispoti, L. A. 2007. An oceanic fixed nitrogen sink exceeding 400 Tg Na-1 vs the concept of homeostasis in the fixed-nitrogen inventory. Biogeosciences **4:** 233–253, doi:10.5194/bg-4-233-2007

Common Wadden Sea Secretariat. 2008. Nomination of the Dutch-German Wadden Sea as world heritage site, v. 1 [Internet]. Wilhelmshaven: Common Wadden Sea Secretariat [accessed 2010 November 3]. p. 21–28. Available from http://www.waddensea-secretariat.org/management/whs/WHS-Final-Dossier(08-01-16).pdf

Cook, P. L. M., and others. 2006. Quantification of denitrification in permeable sediments: Insights from a two-dimensional simulation analysis and experimental data. Limnol. Oceanogr.: Methods **4:** 294–307, doi:10.4319/lom.2006.4.294

De Beer, D., and others. 2005. Transport and mineralization rates in North Sea sandy intertidal sediments, Sylt-Romo Basin, Wadden Sea. Limnol. Oceanogr. **50:** 113–127, doi:10.4319/lo.2005.50.1.0113

Deutsch, B., S. Froster, M. Wilhelm, J. W. Dippner, and M. Voss. 2010. Denitrification in sediments as a major nitrogen sink in the Baltic Sea: An extrapolation using sediment characteristics. Biogeosciences **7:** 3259–3271, doi:10.5194/bg-7-3259-2010

Devol, A. H. 1991. Direct measurement of nitrogen gas fluxes from continental-shelf sediments. Nature **349:** 319–321, doi:10.1038/349319a0

———, L. A. Codispoti, and J. P. Christensen. 1997. Summer and winter denitrification rates in western Arctic shelf sediments. Cont. Shelf Res. **17:** 1029–1050, doi:10.1016/S0278-4343(97)00003-4

Emery, K. O. 1968. Relict sands on continental shelves of the world. AAPG Bull. **52:** 445–464.

Eyre, B. D., and A. J. P. Ferguson. 2002. Comparison of carbon production and decomposition, benthic nutrient fluxes and denitrification in seagrass, phytoplankton, benthic microalgae- and macroalgae-dominated warm-temperate Australian lagoons. Mar. Ecol. Prog. Ser. **229:** 43–59, doi:10.3354/meps229043

Galloway, J. N., and others. 2004. Nitrogen cycles: Past, present, and future. Biogeochemistry **70:** 153–226, doi:10.1007/s10533-004-0370-0

Gao, H., and others. 2010. Aerobic denitrification in permeable Wadden Sea sediments. ISME J. **4:** 417–426, doi:10.1038/ismej.2009.127

Gihring, T. M., A. Canion, A. Riggs, M. Huettel, and J. E. Kostka. 2010. Denitrification in shallow, sublittoral Gulf of Mexico permeable sediments. Limnol. Oceanogr. **55:** 43–54, doi:10.4319/lo.2010.55.1.0043

Gruber, N. 2004. The dynamics of the marine nitrogen cycle and its influence on atmospheric CO_2 variation, p. 97–148. *In* E. M. Follows and T. Oguz [eds.], The ocean carbon cycle and climate. Kluwer Academic.

———. 2008. The marine nitrogen cycle: Overview and challenges, p. 32–35. *In* D. G. Capone, D. Bronk, M. Mulholland, and E. J. Carpenter [eds.], Nitrogen in the marine environment, 2nd ed. Academic Press/Elsevier.

Grunwald, M., and others. 2010. Nutrient dynamics in a back barrier tidal basin of the Southern North Sea: Time-series, model simulations, and budget estimates. J. Sea Res. **64:** 199–212, doi:10.1016/j.seares.2010.02.008

———, O. Dellwig, G. Liebezeit, B. Schnetger, R. Reuter, and H. J. Brumsack. 2007. A novel time-series station in the Wadden Sea (NW Germany): First results on continuous nutrient and methane measurements. Mar. Chem. **107:** 411–421, doi:10.1016/j.marchem.2007.04.003

Guo, Z., and T. S. Zhao. 2002. Lattice Boltzmann model for incompressible flows through porous media. Phys. Rev. E **66:** 036304, doi:10.1103/PhysRevE.66.036304

Hauck, R. D., S. W. Melsted, and P. E. Yankwich. 1958. Use of N-isotope distribution in nitrogen gas in the study of denitrification. Soil Sci. **86:** 287–291, doi:10.1097/00010694-195811000-00011

Holtappels, M., G. Lavik, M. M. Jensen, and M. M. M. Kuypers. 2011. ^{15}N-Labeling experiments to dissect the contributions of heterotrophic denitrification and anammox to nitrogen removal in the OMZ waters of the ocean, p. 223–251. *In* M. G. Klotz [ed.], Methods in enzymology, v. 486. Elsevier Academic Press.

Huettel, M., W. Ziebis, and S. Forster. 1996. Flow-induced uptake of particulate matter in permeable sediments. Limnol. Oceanogr. **41:** 309–322, doi:10.4319/lo.1996.41.2.0309

———, ———, ———, and G. W. Luther. 1998. Advective transport affecting metal and nutrient distributions and interfacial fluxes in permeable sediments. Geochim. Cosmochim. Acta **62:** 613–631, doi:10.1016/S0016-7037(97)00371-2

Jahnke, R. A., S. R. Emerson, and J. W. Murray. 1982. A model of oxygen reduction, denitrification, and organic matter mineralization in marine sediments. Limnol. Oceanogr. **27:** 610–623, doi:10.4319/lo.1982.27.4.0610

Jansen, S., E. Walpersdorf, U. Werner, M. Billerbeck, M. Böttcher, and D. De Beer. 2009. Functioning of intertidal flats inferred from temporal and spatial dynamics of O_2, H_2S and pH in their surface sediment. Ocean Dynam. **59:** 317–332, doi:10.1007/s10236-009-0179-4

Janssen, F. 2004. Pore-water advection and organic matter mineralization in North Sea shelf sands. Ph.D. dissertation. Univ. of Bremen.

Johnson, H. D., and C. T. Baldwin. 1986. Shallow siliciclastic seas, p. 229–282. *In* H. G. Reading [ed.], Sedimentary environments and facies, 2nd ed. Blackwell Scientific Publications.

Kampmeyer, P. M. 1952. The temperature dependence of viscosity for water and mercury. J. Appl. Phys. **23:** 99–102, doi:10.1063/1.1701986

Kieskamp, W.M.L.L., E. Epping, and W. Helder. 1991. Seasonal variation in denitrification rates and nitrous oxide fluxes in intertidal sediments of the western Wadden Sea. Mar. Ecol. Prog. Ser. **72:** 145–151, doi:10.3354/meps072145

Laursen, A. E., and S. P. Seitzinger. 2002. The role of denitrification in nitrogen removal and carbon mineralization in Mid-Atlantic Bight sediments. Cont. Shelf Res. **22:** 1397–1416, doi:10.1016/S0278-4343(02)00008-0

Lohse, L., H. T. Kloosterhuis, W. van Raaphorst, and W. Helder. 1996. Denitrification rates as measured by the isotope pairing method and by the acetylene inhibition technique in continental shelf sediments of the North Sea. Mar. Ecol. Prog. Ser. **132:** 169–179, doi:10.3354/meps132169

Nielsen, L. P. 1992. Denitrification in sediment determined from nitrogen isotope pairing. FEMS Microbiol. Ecol. **86:** 357–362, doi:10.1111/j.1574-6968.1992.tb04828.x

———, and R. N. Glud. 1996. Denitrification in a coastal sediment measured in situ by isotope paring applied to a benthic flux chamber. Mar. Ecol. Prog. Ser. **137:** 181–186, doi:10.3354/meps137181

Perry, R. H., and D. Green. 1984. Physical and chemical data, p. 3-248–3-252. *In* Perry's chemical engineers' handbook, 6th ed. McGraw-Hill.

Precht, E., and M. Huettel. 2003. Advective pore-water exchange driven by surface gravity waves and its ecological implications. Limnol. Oceanogr. **48:** 1674–1684, doi:10.4319/lo.2003.48.4.1674

———, and ———. 2004. Rapid wave-driven advective pore water exchange in a permeable coastal sediment. J. Sea Res. **51:** 93–107, doi:10.1016/j.seares.2003.07.003

Rao, A. M. F., M. J. McCarthy, W. S. Gardner, and R. A. Jahnke. 2007. Respiration and denitrification in permeable continental shelf deposits on the South Atlantic Bight: Rates of carbon and nitrogen cycling from sediment column experiments. Cont. Shelf Res. **27:** 1801–1819, doi:10.1016/j.csr.2007.03.001

———, ———, ———, and ———. 2008. Respiration and denitrification in permeable continental shelf deposits on the South Atlantic Bight: N-2 : Ar and isotope pairing measurements in sediment column experiments. Cont. Shelf Res. **28:** 602–613, doi:10.1016/j.csr.2007.11.007

Reimers, C. E., and others. 2004. In situ measurements of advective solute transport in permeable shelf sands. Cont. Shelf Res. **24:** 183–201, doi:10.1016/j.csr.2003.10.005

Rusch, A., and M. Huettel. 2000. Advective particle transport into permeable sediments—evidence from experiments in an intertidal sandflat. Limnol. Oceanogr. **45:** 525–533, doi:10.4319/lo.2000.45.3.0525

Seeberg-Elverfeldt, J., M. Schlüter, T. Feseker, and M. Kölling. 2005. Rhizon sampling of porewaters near the sediment–water interface of aquatic systems. Limnol. Oceanogr.: Methods **3:** 361–371, doi:10.4319/lom.2005.3.361

Shaffer, G., and U. Rönner. 1984. Denitrification in the Baltic Proper deep-water. Deep-Sea Res. **31:** 197–220.

Thamdrup, B., and T. Dalsgaard. 2002. Production of N_2 through anaerobic ammonium oxidation coupled to nitrate reduction in Marine sediments. Appl. Environ. Microbiol. **68:** 1312–1318, doi:10.1128/AEM.68.3.1312-1318.2002

———, and ———. 2008. Nitrogen cycling in sediments, p. 527–568. *In* E. D. L. Kirchman [ed.], Microbial ecology of the oceans, 2nd ed. John Wiley & Sons.

Trimmer, M., and J. C. Nicholls. 2009. Production of nitrogen gas via anammox and denitrification in intact sediment cores along a continental shelf to slope transect in the North Atlantic. Limnol. Oceanogr. **54:** 577–589, doi:10.4319/lo.2009.54.2.0577

Tuominen, L., A. Heinanen, J. Kuparinen, and L. P. Nielsen. 1998. Spatial and temporal variability of denitrification in the sediments of the northern Baltic Proper. Mar. Ecol. Prog. Ser. **172:** 13–24, doi:10.3354/meps172013

van Beusekom, J. E. E., H. Fock, F. de Jong, S. Diel-Christiansen, and B. Christiansen. 2001. Wadden Sea specific eutrophication criteria. Wadden Sea Ecosystem No. 14. Common Wadden Sea Secretariat.

———, S. Weigelt-Krenz, and P. Martens. 2008. Long-term variability of winter nitrate concentrations in the Northern Wadden Sea driven by freshwater discharge, decreasing riverine loads and denitrification. Helgol. Mar. Res. **62:** 49–57, doi:10.1007/s10152-007-0092-5

Vance-Harris, C., and E. Ingall. 2005. Denitrification pathways and rates in the sandy sediments of the Georgia continental shelf, USA. Geochem. Trans. **6:** 12–18, doi:10.1186/1467-4866-6-12

Associate editor: Bo Thamdrup

Received: 21 December 2010
Accepted: 26 July 2011
Amended: 24 September 2011